CARBON letters

Original Articles
Carbon Letters Vol. 12, No. 4, 236-242 (2011)

Influence of oxyfluorination on activated carbon nanofibers for CO_2 storage

Byong Chol Bai[1,2], Jong Gu Kim[2], Ji Sun Im[2], Sang-Chul Jung[3], Young-Seak Lee[1,2,♠]

[1]Department of Green Energy Technology, Chungnam National University, Daejeon 305-764, Republic of Korea
[2]Department of Fine Chemical Engineering and Applied Chemistry, BK21-E2M, Chungnam National University, Daejeon 305-764, Republic of Korea
[3]Department of Environmental Engineering, Sunchon National University, Sunchon 540-742, Republic of Korea

Article Info

Received 20 August 2011
Accepted 21 November 2011

***Corresponding Author**
E-mail: youngslee@cnu.ac.kr
Tel: +82-42-821-7007

Open Access
DOI: http://carbonlett.org/10.5714/CL.2011.12.4.236

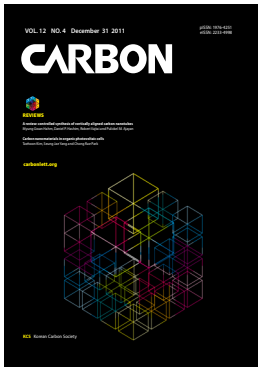

http://carbonlett.org

pISSN: 1976-4251
eISSN: 2233-4998

Abstract

The oxyfluorination effects of activated carbon nanofibers (OFACFs) were investigated for CO_2 storage. Electrospun CFs were prepared from a polyacrylonitrile/*N*,*N*-dimethylformamide solution via electrospinning and heat treatment. The electrospun CFs were chemically activated in order to generate the pore structure, and then oxyfluorination was used to modify the surface. The samples were labeled CF (electrospun CF), ACF (activated CF), OFACF-1 (O_2:F_2 = 7:3), OFACF-2 (O_2:F_2 = 5:5) and OFACF-3 (O_2:F_2 = 3:7). The functional group of OFACFs was investigated using X-ray photoelectron spectroscopy analysis. The C-F bonds formed on surface of ACFs. The intensities of the C-O peaks increased after oxyfluorination and increased the oxygen content in the reaction gas. The specific surface area, pore volume and pore size of OFACFs were calculated by the Brunauer–Emmett–Teller and density functional theory equation. Through the N_2 adsorption isotherm, the specific surface area and pore volume slightly decreased as a result of oxyfluorination treatment. Nevertheless, the CO_2 adsorption efficiency of oxyfluorinated ACF improved around 16 wt% due to the semi-ionic interaction effect of surface modificated oxygen functional groups and CO_2 molecules.

Key words: carbon nanofibers, CO_2 storage, porosity, oxyfluorination, electrospun

1. Introduction

Emissions from the combustion of fossil fuels are contributing to an increase in the concentration of carbon dioxide (CO_2) in the atmosphere. It is generally accepted that this increase in atmospheric CO_2 may be causing global climate change. Researchers have reported that global CO_2 emissions from fossil fuels increased 29% between 2000 and 2008 and 41% between 1990 and 2008. According to a new study, the current concentration of CO_2 in the atmosphere is at its highest now in at past 2 million years [1]. Consequently, CO_2 capture from large point sources has recently received attention as a potential means of mitigating fossil fuel CO_2 emissions. Current or proposed methods for capturing CO_2 from flue gas have included absorption, adsorption, cryogenic distillation, and membrane separation. However, commercial CO_2 capture technology existing today is very expensive and energy intensive. Improving the technologies for CO_2 adsorption is necessary in order to achieve low-energy rewards [2].

CO_2 adsorption is typically used as a final polishing step in a hybrid CO_2 capture system [3]. Ideally, CO_2 adsorbents should have the following characteristics: a high specific surface area, well developed micro- and mesopores, and many active sites on the surfaces, such as amine functional groups and basic metal oxides [4-6]. Up to the present, different types of adsorbents have been used for CO_2 adsorption, such as zeolites, alumina, mesoporous silica,

CaO, and porous carbons [7-11]. In particular, porous carbons have been preferred for CO_2 adsorption due to their highly developed porosity, extended surface area, surface chemistry, and thermal stability. Previous studies have also used activated carbons, activated carbon fibers (ACF), carbon molecular sieves, and carbon nanotubes as adsorbents for CO_2 adsorption [12-14].

In general, the adsorption capacity on porous carbon materials depends on the surface area and pore structures of adsorbents. Additionally, the surface carbon/adsorbates interactions have an influence on the adsorption capacity [15-17]. Surface modification is able to change this interaction, and numerous surface modification methods have been published in the literature. Of these methods, fluorination is one of the most effective methods for modifing carbon surfaces [18-21]. Because fluorine gas has a strong reactivity, it can easily react with surface carbon, even at room temperature. Furthermore, the surface nature of activated carbons can be controlled, regardless of whether they are hydrophobic or hydrophilic, by direct fluorination and oxyfluorination [22].

We modified activated electrospun CFs with fluorine gas, and characterized the changes in its surface properties and pore structure before and after oxyfluorination. Afterwards, we investigated the interaction of adsorbent–adsorbate from CO_2 adsorption isotherms of oxyfluorinated activated electrospun CFs at 273 K. From these results, we determined the relationship between the storage capacity and the pore structures of the ACF samples. This paper reports our preliminary results on the catalytic effect of ACFs modified by F_2 and its potential benefits.

2. Experimental Methods

2.1. Materials

Polyacrylonitrile (PAN, d = 1.184, Aldrich) was used as a carbon source. N,N-dimethyl formamide (DMF) was adopted as a solvent, because its boiling point is 426 K and it has a conductivity (conductivity = 10.90 μS/cm, dipole moment = 3.82 Debye) sufficiently high for electrospinning. In order to develop the pore structure, potassium hydroxide (KOH) was used as a chemical activation agent. Fluorine (Messer Grieheim GmbH, 99.8%) and oxygen (99.99%) gases were used for the oxyfluorination treatment [23,24]. The prepared polymer solution (PAN/DMF, 10 wt%) was ejected from a syringe tip onto an aluminum-foil-covered collector using an electrospinning apparatus. A schematic diagram of the electrospinning apparatus was depicted in our previous paper [25]. Electrospinning was performed under the following conditions: feeding rate of polymer solution: 1 mL/h; supplied voltage: 18 kV; tip to collector distance: 10 cm; collector rpm: 150. The stabilization of the electrospun materials was carried out in air by heating up to 523 K at a heating rate of 1 K/min, and finally, samples were treated at 523 K for 8 h. Carbonization of the stabilized electrospun materials was carried out under a nitrogen atmosphere with the following conditions to carbonize the oxidized fibers: heating rate: 10 K/min; reaction temperature: 1323 K; holding time: 1 h nitrogen feeding rate: 100 mL/h [26]. The final product is called an electrospun carbon fiber in this study.

The KOH solutions (6 M) were prepared as chemical activation agents. The CF sample was placed on an alumina boat at a ratio of 10 mL/g (KOH solution/CF) in a steel pipe to carry out the chemical activation. Activation was conducted at 1023 K for 3 h in an argon atmosphere. The heating rate was 5 K/min, and the feed rate of the argon gas was 40 mL/min. After chemical activation, samples were washed with distilled water several times to remove residual potassium. These were then dried at 383 K overnight. These activated carbon nanofibers are called ACF.

2.2. Surface modification by oxyfluorination of ACFs

As a pretreatment step, ACFs were heated at 70°C for 24 h to remove impurities. The oxyfluorination was carried out at 1 bar for 5 min with oxygen:fluorine gas ratios of 7:3, 5:5 and 3:7. These oxyfluorinated samples are labeled oxyfluorination effects of activated carbon nanofiber (OFACF)-1 (O_2:F_2 = 7:3), OFACF-2 (O_2:F_2 = 5:5) and OFACF-3 (O_2:F_2 = 3:7). More details on this reaction are provided in a previous study [26].

2.3. Characterization of prepared samples

The X-ray photoelectron spectroscopy (XPS) spectra of the samples were obtained using a MultiLab 2000 spectrometer (Thermo Electron Corporation, England) in order to investigate the elements present in the samples. Al Ka (1485.6 eV) was used as the X-ray source with a 14.9-keV anode voltage, a 4.6-A filament current and a 20-mA emission current. All samples were treated at 10^{-9} mbar to remove impurities. The survey spectra were obtained at a 50-eV pass energy and a 0.5-eV step size.

The textural properties of the all the samples were investigated. Samples were degassed at 423 K for 3 h, and then, nitrogen adsorption was carried out at 77 K using a Brunauer–Emmett–Teller (BET) apparatus (Micromeritics ASAP 2020) to investigate the specific surface area, total pore volume, pore size distribution and micropore fraction.

The CO_2 adsorption capacity was measured by CO_2 isothermal adsorption at 273 K and 1 atm. Furthermore, the parameters of the Dubinin–Astakhov equation:

$$\log(V) = \log(V_0) - \left[\frac{RT}{\beta E_0}\right]^n \left[\log\left(\frac{p_0}{p}\right)\right]^n$$

were obtained from CO_2 adsorption. p, p_0, V, V_0, n, R, E_0, and β are the equilibrium pressure, the saturation vapor pressure of the gas at the analysis temperature (T), the volume adsorbed at equilibrium pressure, the monolayer capacity, the Astakhov exponent, the gas constant, characteristic energy, and the affinity coefficient of the analysis gas, respectively.

3. Results and Discussion

3.1. Surface properties of oxyfluorinated ACFs

XPS analysis was very useful for characterizing the surface chemical structures of the oxyfluorinated ACFs in the previous

Table 1. XPS surface element analysis of as-received and OFACFs

Samples	C1s	O1s	F1s	O1s/C1s (atomic ratio/%)	F1s/C1s (atomic ratio/%)	$C_xO_yF_z$
	Atomic percent (at%)	Atomic percent (at%)	Atomic percent (at%)			
ACF	94.72	5.28	-	5.57	-	$C_{10}O_{0.56}$
OFACF-1	91.73	6.89	1.38	7.51	1.50	$C_{10}O_{0.75}F_{0.15}$
OFACF-2	88.28	10.13	1.59	11.47	1.80	$C_{10}O_{1.15}F_{0.18}$
OFACF-3	91.10	6.35	2.55	6.97	2.80	$C_{10}O_{0.70}F_{0.28}$

XPS: X-ray photoelectron spectroscopy, OFACF: oxyfluorinated activated carbon nanofiber.

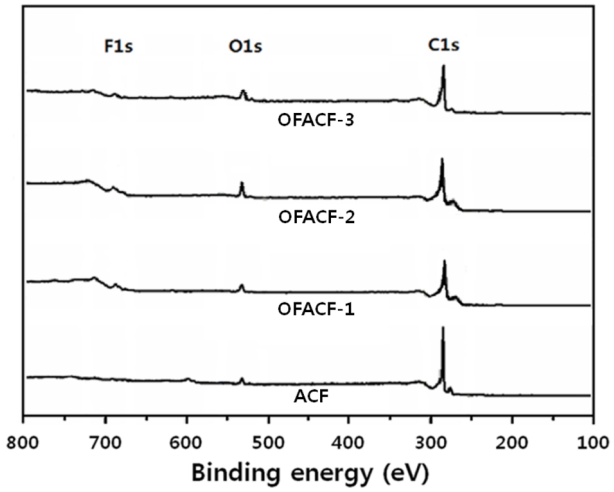

Fig. 1. Elemental-survey data of the un-oxyfluorinated and oxyfluorinated activated carbon nanofibers (OFACFs).

studies [27-29]. Characterization of the surface chemical composition of the oxyfluorinated ACFs was carried out using XPS analysis. Table 1 lists the atomic ratio of each element on the surface of the ACFs. The surface carbon concentration of the samples decreased dramatically after oxyfluorination, whereas the fluorine atomic ratio of the samples significantly increased. In addition, the O_{1s} peaks of the oxyfluorinated ACFs slightly increased with the decrease in fluorine partial pressure, but the O_{1s} peak of sample OFACF-3 decreased because there was insufficient fluorine gas to react with the oxygen gas.

Fig. 1 shows the elemental survey of pristine and oxyfluorinated ACFs. In the ACF sample, C_{1s} and O_{1s} peaks represent the carbon atoms from ACFs and the oxygen atoms from the H_2O adsorption on ACFs from the ambient atmosphere, respectively. The peaks of O_{1s} and F_{1s} confirmed the introduction of both oxygen and fluorine atoms, respectively, on the oxyfluorinated ACFs. The peak intensities varied depending on the composition of the reactive gases. In the C1s spectra of oxyfluorinated ACFs, the peak intensity increased with decreasing fluorination pressure. Fluorine gas appeared to react with the carbon more actively than with the oxygen, resulting in the breakage of the sp^2 carbon aromatic structure. The carbon-oxygen single and double-bond peak intensities increased with increasing oxygen content in the reactive gas [30]. In sample OFACF-2, the total content of carbon-oxygen single and double bonds increased by over 20%. These carbon–oxygen bonds contributed to the increased hydrophilicity of the ACFs; while in the OFACF-3 sample, the total content of carbon-oxygen single- and double-bonds decreased because there was insufficient fluorine gas to react with the oxygen gas. The fluorinated carbon bonds were observed as semi-ionic and covalent carbon-fluorine bonds [31]. Even though the intensities of all of the fluorinated carbon bonds increased as the fluorine content in the reactive gas increased, the covalent carbon-fluorine bond was dominant.

The O_{1s} and F_{1s} peaks were also investigated as supplementary data for interpreting the C_{1s} peaks. The variation in the O_{1s} peaks corresponded well with the variation of the C_{1s} peaks upon oxyfluorination. The carbon-oxygen single and double bonds were produced more favorably by oxyfluorination. The variation in the F_{1s} peaks also corresponded well with the variation of the C_{1s} peaks upon oxyfluorination. The covalent carbon-fluorine bonds were more dominant when the fluorine content in the reactive gas was increased.

The changes in the chemical bonds of the ACFs after oxyfluorination were investigated by C_{1s} deconvolution, and the results are depicted in Fig. 2. Table 2 lists the C_{1s} spectra and assignments of the oxyfluorinated ACFs. The C_{1s} peaks of oxyfluorinated ACFs was deconvoluted to several pseudo-Voigt functions (sums of the Gaussian and Lorentzian functions) using a peak-analysis program obtained from Unipress Co., USA. The pseudo-Voigt function is given by [32]:

$$F(E) = H\left[(1-S)\exp\left(-\ln(2)\left(\frac{E-E_0}{FWHM}\right)^2\right) + \frac{S}{1+\left(\frac{E-E_0}{FWHM}\right)^2}\right]$$

where F(E) is the intensity at energy E, H is the peak height, E_0 is the peak center and S is a shape function related to the symmetry and the Gaussian–Lorentzian mixing ratio. The components observed for ACF were C(1), C(2), C(3), and C(4) at 284.5, 285.7, 286.9, and 288.1 eV, corresponding respectively to the sp^2 carbon, sp^3 carbon, carbon-oxygen single- and double-bonds. After oxyfluorination, the C(5) and C(6) components were observed in OFACF-1, OFACF-2, and OFACF-3 samples at 289.3 and 290.5 eV, corresponding to semi-covalent and covalent carbon-fluorine, respectively. All of these results are in accord with those from other studies [19,21,27-29,33-35]. The concentration of C(3) and C(4) increased as the O_2 to F_2 ratio increased in the gas mixture, whereas the ratio only decreased in the OFACF-3 sample because there was insufficient fluorine gas to react with

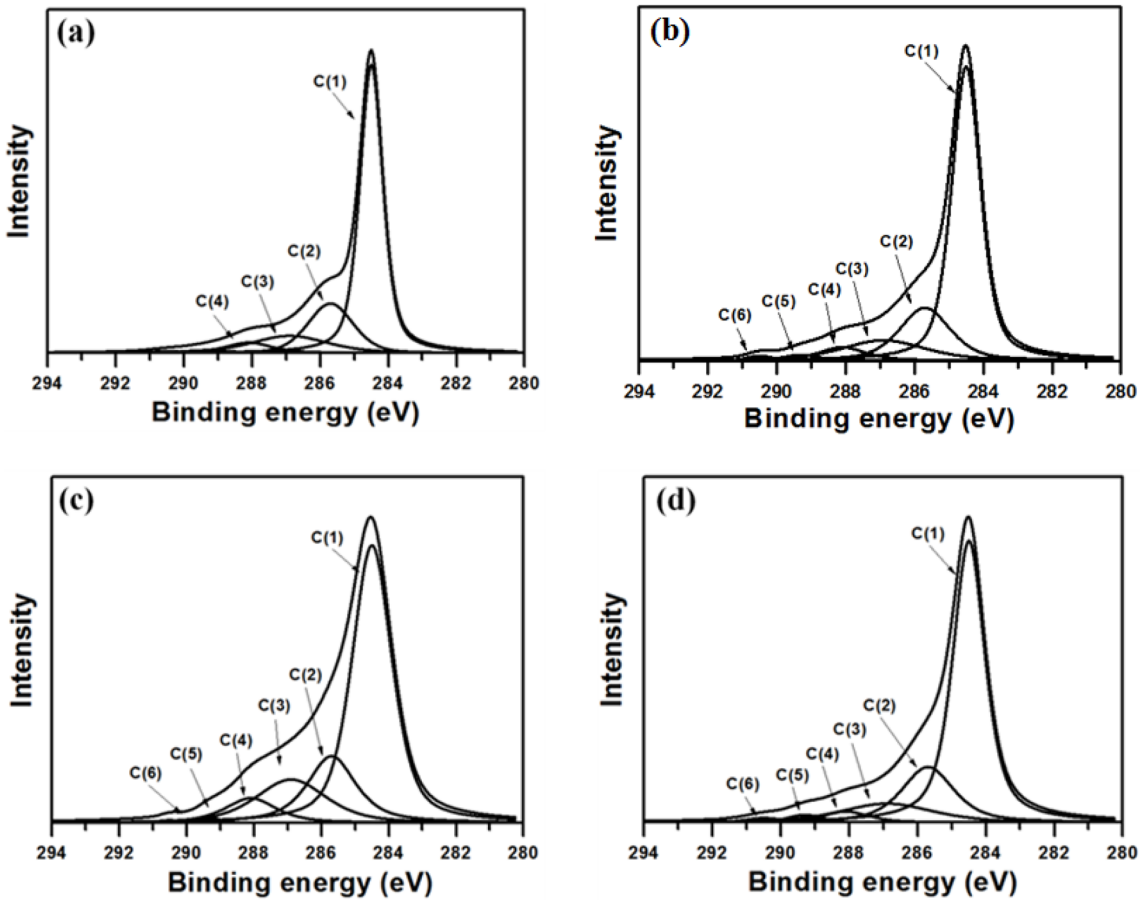

Fig. 2. C1s deconvolution of the un-oxyfluorinated and oxyfluorinated activated carbon nanofibers (OFACFs). (a) ACF, (b) OFACF-1, (c) OFACF-2, and (d) OFACF-3.

Table 2. C1s spectra and assignment of the OFACFs

Component	Binding energy (eV)	Assignment	Concentration (%) of samples			
			ACF	OFACF-1	OFACF-2	OFACF-3
C(1)	284.5	C-C (sp^2)	77.17	61.22	57.99	62.59
C(2)	285.7	C-C (sp^3)	15.03	19.21	18.28	19.62
C(3)	286.9	C-O	5.87	12.31	15.94	11.48
C(4)	288.1	C=O	1.93	4.93	7.02	3.47
C(5)	289.3	Semi-ionic C-F	-	1.49	0.53	1.69
C(6)	290.5	Covalent C-F	-	0.84	0.24	1.15

OFACF: oxyfluorinated activated carbon nanofiber.

the oxygen gas, as previously mentioned. However, C(5) and C(6) decreased with a decreasing F_2 ratio in the gas. The effect of the functional groups discussed in this section will be further discussed in later sections.

3.2. Textural properties

A summary of the textural properties is presented in Table 3. KOH activation has the effect of increasing specific surface area, total pore volume, and micropore volume while increasing the concentration of the used chemical agent solution. The nitrogen isotherms of the samples are shown in Fig. 3. All of the curves have an inflection point, which is called a 'knee,' around P/P_0 (0.01). This point indicates that monolayer adsorption is complete. Thus, it is possible to calculate the specific surface area at this point using the BET equation. Generally, in the low-pressure region, less than around 0.1 P/P_0, the steep curve of the isotherm indicates the development of the micropore struc-

Table 3. Textural properties of the un-oxyfluorinated and OFACFs

Sample	S_{BET} (m^2/g)[a]	V_T (cm^3/g)[b]	V_M (cm^3/g)[c]
ACF	1239	0.437	0.432
OFACF-1	1181	0.401	0.399
OFACF-2	1121	0.386	0.390
OFACF-3	1179	0.398	0.395

OFACF: oxyfluorinated activated carbon nanofiber.
[a] S_{BET} : Brunauer–Emmett–Teller-specific surface area.
[b] V_T : total pore volume.
[c] V_M : t-plot micropore volume.

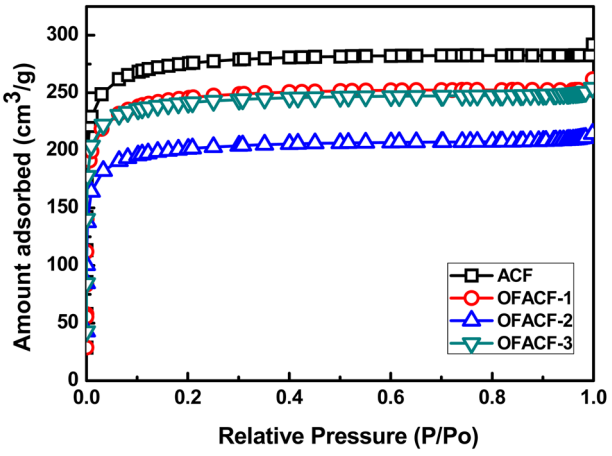

Fig. 3. Adsorption isotherms of nitrogen on the un-oxyfluorinated and oxyfluorinated activated carbon nanofibers (OFACFs).

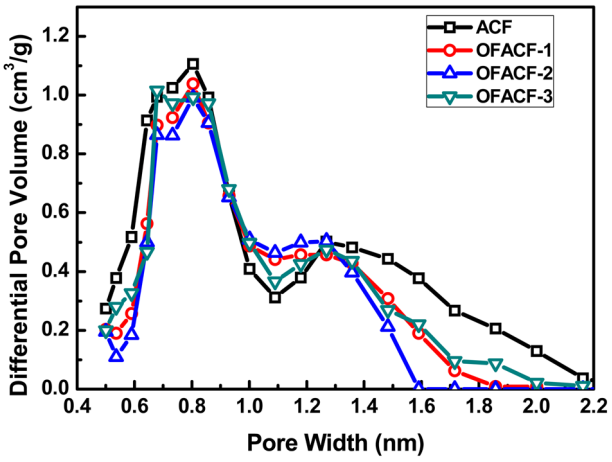

Fig. 4. Non-local density functional theory pore size distribution. OFACF: oxyfluorinated activated carbon nanofiber.

ture, and the change in the relatively high-pressure region indicates the improvement of meso/macro pores [36]. In the case of OFACF-1, OFACF-2 and OFACF-3, a well-developed microporous property was confirmed by the striking initial change in the low relative pressure range [37]. In our previous work, it was shown that KOH activated carbon nanofibers have highly developed micropores, and oxyfluorination treatment of ACFs does not significantly affect the pore structure under the conditions used [26].

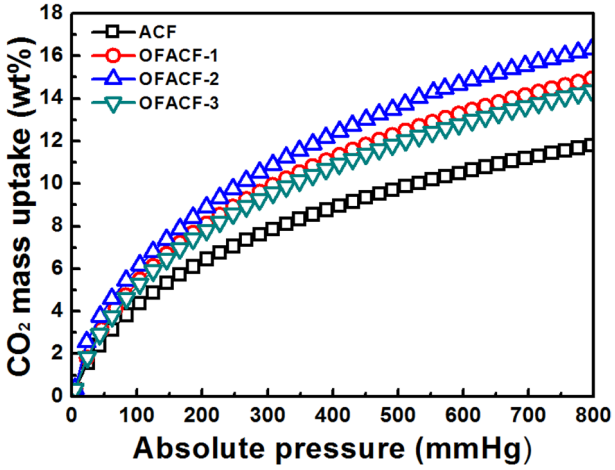

Fig. 5. Adsorption equilibrium isotherms of CO_2 on all samples. OFACF: oxyfluorinated activated carbon nanofiber.

The pore size distribution was evaluated by applying a non-local density functional theory (NLDFT) model, as shown in Fig. 4. The NLDFT model was applied under the assumption that the slit-shaped pores have uniformly dense carbon walls and that the adsorbate is a fluid of hard spheres [38]. Additionally, the interaction between adsorbent and adsorbate was considered on their elemental species by a soft program installed on the BET apparatus. The pore width was distributed mainly in the micopore range, especially in the range of 0.7-1.6 nm. Based on the information provided by other groups, this pore size distribution would be very beneficial for CO_2 uptake, because it has been predicted that the optimized pore size for enhancing the capacity of CO_2 storage in carbon materials is 0.8-1.1 nm [39,40].

3.3. Capacity of CO_2 uptake

Adsorption equilibrium isotherms of CO_2 on all samples at 273 K are plotted in Fig. 5. It can be seen that the OFACFs had a better performance in CO_2 adsorption than the pristine ACFs. This may occur because the filling of micropores with CO_2 gas is increase at that pressure [41]. This clearly indicates that modification by KOH activation and oxyfluorination treatment increase the affinity of ACFs toward CO_2. Comparing ACFs, a higher CO_2 uptake can be observed in the case of OFACF-2. The cause is surely the more highly-developed pore structure. Based on the investigation of oxyfluorination effects for enhancing CO_2 storage, the CO_2 uptake of the oxyfluorinated samples was studied. In all pressure ranges, oxyfluorination effects can be observed, showing a higher capacity of CO_2 uptake than raw ACF. It is around 11% (OFACF-1 and OFACF-3) and 30% (OFACF-2) higher, as compared with ACF sample, respectively. Overall, the CO_2 uptakes of the samples were 11.2 (ACF), 14.2 (OFACF-1), 16.2 (OFACF-2) and 13.9 wt% (OFACF-3).

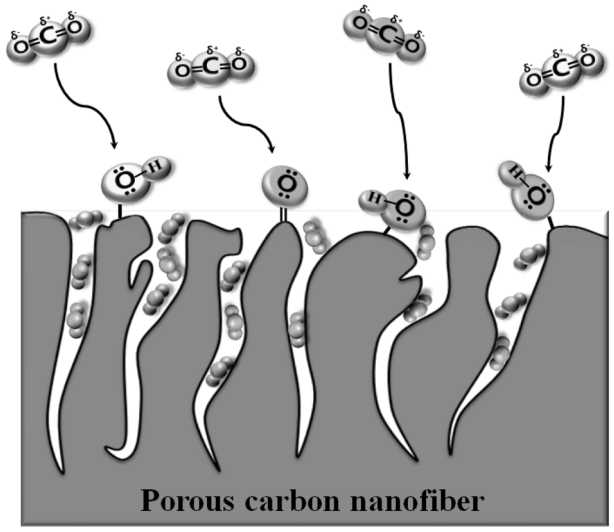

Fig. 6. Suggested mechanism for the improved effects of oxyfluorinated activated carbon nanofibers.

3.4. Suggested mechanism for the improved effects of oxyfluorinated ACFs

The mechanism of CO_2 storage in the slit pores of oxyfluorinated ACFs is suggested in Fig. 6. The CO_2 molecule has a non-polar structure. The CO_2 molecules near the carbon pores are affected by the semi-ionic interaction of oxygen groups, which has the lone-pair electron, causing the attraction of the electrons in the CO_2 molecules, as shown in Fig. 6. This reaction might play an important role as a guide for enhancing the CO_2 storage capacity. Eventually, the CO_2 gas can be stored in the slit pores of carbon. Some of the residual CO_2 molecules in the carbon silt pores can be also affected by oxygen group effects, such as the grabbing effects due to semi ionic interaction, resulting in the high efficiency of CO_2 storage. All of these reactions were carried out without any chemical bonds between the CO_2 molecules and the carbon pores, so the desorption of CO_2 is easily reversible for ease of use.

4. Conclusions

In conclusion, we have shown that the CO_2 adsorption behaviors of ACFs are directly related to oxyfluorination. Samples were oxyfluorinated for surface modification to investigate the semi-ionic interaction effect of enhancing the capacity of CO_2 storage by oxygen group. The resulting samples were highly microporous, over 85%, with a high specific surface area greater than 1200 m^2/g and a pore size distribution in the range of 0.7-1.6 nm, optimal for CO_2 storage. Eventually, the CO_2 uptake increased up to 16.2 wt% due to the highly developed micropore structure and semi-ionic interaction effect of oxyfluorination.

References

[1] Reay DS, Dentener F, Smith P, Grace J, Feely RA. Global nitrogen deposition and carbon sinks. Nature Geosci, **1**, 430 (2008). http://dx.doi.org/10.1038/ngeo230.

[2] International Energy Agency. Tracking Industrial Energy Efficiency and CO_2 Emissions: In Support of the G8 Plan of Action: Energy Indicators, International Energy Agency, Paris, France (2007).

[3] Aaron D, Tsouris C. Separation of CO_2 from flue gas: a review. Sep Sci Technol, **40**, 321 (2005). http://dx.doi.org/10.1081/ss-200042244.

[4] Meng L, Cho KS, Park SJ. CO_2 adsorption of amine functionalized activated carbons. Carbon Lett, **10**, 221 (2009).

[5] Meng L, Cho KS, Park SJ. Effect of heat treatment on CO_2 adsorption of ammonized graphite nanofibers. Carbon Lett, **11**, 34 (2010).

[6] Kim BJ, Cho KS, Park SJ. Copper oxide-decorated porous carbons for carbon dioxide adsorption behaviors. J Colloid Interface Sci, **342**, 575 (2010). http://dx.doi.org/10.1016/j.jcis.2009.10.045.

[7] Yang H, Xu Z, Fan M, Gupta R, Slimane RB, Bland AE, Wright I. Progress in carbon dioxide separation and capture: a review. J Environ Sci, **20**, 14 (2008). http://dx.doi.org/10.1016/s1001-0742(08)60002-9.

[8] Chatti R, Bansiwal AK, Thote JA, Kumar V, Jadhav P, Lokhande SK, Biniwale RB, Labhsetwar NK, Rayalu SS. Amine loaded zeolites for carbon dioxide capture: amine loading and adsorption studies. Microporous Mesoporous Mater, **121**, 84 (2009). http://dx.doi.org/10.1016/j.micromeso.2009.01.007.

[9] Caixin L, Lei Z, Jiguang D, Qing M, Hongxing D, Hong H. Surfactant-aided hydrothermal synthesis and carbon dioxide adsorption behavior of three-dimensionally mesoporous calcium oxide single-crystallites with tri-, tetra-, and hexagonal morphologies. J Phys Chem C, **112**, 19248 (2008). http://dx.doi.org/10.1021/jp8064568.

[10] Plaza MG, Pevida C, Arias B, Fermoso J, Arenillas A, Rubiera F, Pis JJ. Application of thermogravimetric analysis to the evaluation of aminated solid sorbents for CO_2 capture. J Therm Anal Calorim, **92**, 601 (2008). http://dx.doi.org/10.1007/s10973-007-8493-x.

[11] Siriwardane RV, Shen MS, Fisher EP, Poston JA. Adsorption of CO_2 on molecular sieves and activated carbon. Energy Fuels, **15**, 279 (2001). http://dx.doi.org/10.1021/ef000241s.

[12] Tenney CM, Lastoskie CM. Molecular simulation of carbon dioxide adsorption in chemically and structurally heterogeneous porous carbons. Environ Prog, **25**, 343 (2006). http://dx.doi.org/10.1002/ep.10168.

[13] Moon SH, Shim JW. A novel process for CO_2/CH4 gas separation on activated carbon fibers-electric swing adsorption. J Colloid Interface Sci, **298**, 523 (2006). http://dx.doi.org/10.1016/j.jcis.2005.12.052.

[14] Hu YH, Ruckenstein E. Applicability of Dubinin-Astakhov equation to CO_2 adsorption on single-walled carbon nanotubes. Chem Phys Lett, **425**, 306 (2006). http://dx.doi.org/10.1016/j.cplett.2006.05.059.

[15] Zhao XB, Xiao B, Fletcher AJ, Thomas KM. Hydrogen adsorption on functionalized nanoporous activated carbons. J Phys Chem B, **109**, 8880 (2005). http://dx.doi.org/10.1021/jp050080z.

[16] Celzard A, Perrin A, Albiniak A, Broniek E, Mareche JF. The effect of wetting on pore texture and methane storage ability of NaOH activated anthracite. Fuel, **86**, 287 (2007). http://dx.doi.org/10.1016/j.fuel.2006.05.033.

[17] Chingombe P, Saha B, Wakeman RJ. Surface modification and characterisation of a coal-based activated carbon. Carbon, **43**, 3132 (2005). http://dx.doi.org/10.1016/j.carbon.2005.06.021.

[18] Touhara H, Okino F. Property control of carbon materials by fluorination. Carbon, **38**, 241 (2000). http://dx.doi.org/10.1016/s0008-6223(99)00140-2.

[19] Lee YS. Syntheses and properties of fluorinated carbon materials. J Fluorine Chem, **128**, 392 (2007). http://dx.doi.org/10.1016/j.jfluchem.2006.11.014.

[20] Tressaud A, Durand E, Labrugere C. Surface modification of several carbon-based materials: comparison between CF4 rf plasma and direct F2-gas fluorination routes. J Fluorine Chem, **125**, 1639 (2004). http://dx.doi.org/10.1016/j.jfluchem.2004.09.022.

[21] Lee YS, Lee BK. Surface properties of oxyfluorinated PAN-based carbon fibers. Carbon, **40**, 2461 (2002). http://dx.doi.org/10.1016/s0008-6223(02)00152-5.

[22] Lee YS, Kim YH, Hong JS, Suh JK, Cho GJ. The adsorption properties of surface modified activated carbon fibers for hydrogen storages. Catal Today, **120**, 420 (2007). http://dx.doi.org/10.1016/j.cattod.2006.09.014.

[23] Im JS, Park SJ, Kim T, Lee YS. Hydrogen storage evaluation based on investigations of the catalytic properties of metal/metal oxides in electrospun carbon fibers. Int J Hydrogen Energy, **34**, 3382 (2009). http://dx.doi.org/10.1016/j.ijhydene.2009.02.047.

[24] Im JS, Yun J, Lim YM, Kim HI, Lee YS. Fluorination of electrospun hydrogel fibers for a controlled release drug delivery system. Acta Biomater, **6**, 102 (2010). http://dx.doi.org/10.1016/j.actbio.2009.06.017.

[25] Im JS, Park SJ, Lee YS. Preparation and characteristics of electrospun activated carbon materials having meso- and macropores. J Colloid Interface Sci, **314**, 32 (2007). http://dx.doi.org/10.1016/j.jcis.2007.05.033.

[26] Im JS, Park SJ, Lee YS. The metal-carbon-fluorine system for improving hydrogen storage by using metal and fluorine with different levels of electronegativity. Int J Hydrogen Energy, **34**, 1423 (2009). http://dx.doi.org/10.1016/j.ijhydene.2008.11.054.

[27] Ho KKC, Lee AF, Bismarck A. Fluorination of carbon fibres in atmospheric plasma. Carbon, **45**, 775 (2007). http://dx.doi.org/10.1016/j.carbon.2006.11.015.

[28] Bismarck A, Tahhan R, Springer J, Schulz A, Klapotke TM, Zell H, Michaeli W. Influence of fluorination on the properties of carbon fibres. J Fluorine Chem, **84**, 127 (1997). http://dx.doi.org/10.1016/S0022-1139(97)00029-8.

[29] Tressaud A, Durand E, Labrugere C, Kharitonov AP, Kharitonova LN. Modification of surface properties of carbon-based and polymeric materials through fluorination routes: from fundamental research to industrial applications. J Fluorine Chem, **128**, 378 (2007). http://dx.doi.org/10.1016/j.jfluchem.2006.12.015.

[30] Park SJ, Kim BJ. Ammonia removal of activated carbon fibers produced by oxyfluorination. J Colloid Interface Sci, **291**, 597 (2005). http://dx.doi.org/10.1016/j.jcis.2005.05.012.

[31] Chamssedine F, Claves D. Selective substitution of fluorine atoms grafted to the surface of carbon nanotubes and application to an oxyfluorination strategy. Carbon, **46**, 957 (2008). http://dx.doi.org/10.1016/j.carbon.2008.03.001.

[32] Kauffman DR, Sorescu DC, Schofield DP, Allen BL, Jordan KD, Star A. Understanding the sensor response of metal-decorated carbon nanotubes. Nano Lett, **10**, 958 (2010). http://dx.doi.org/10.1021/nl903888c.

[33] Xu B, Wang X, Lu Y. Surface modification of polyacrylonitrile-based carbon fiber and its interaction with imide. Appl Surf Sci, **253**, 2695 (2006). http://dx.doi.org/10.1016/j.apsusc.2006.05.044.

[34] Crassous I, Groult H, Lantelme F, Devilliers D, Tressaud A, Labrugere C, Dubois M, Belhomme C, Colisson A, Morel B. Study of the fluorination of carbon anode in molten KF-2HF by XPS and NMR investigations. J Fluorine Chem, **130**, 1080 (2009). http://dx.doi.org/10.1016/j.jfluchem.2009.07.022.

[35] Ma K, Chen P, Wang B, Cui G, Xu X. A study of the effect of oxygen plasma treatment on the interfacial properties of carbon fiber/epoxy composites. J Appl Polym Sci, **118**, 1606 (2010). http://dx.doi.org/10.1002/app.32549.

[36] Gregg SJ, Sing KSW. Adsorption, Surface Area, and Porosity. 2nd ed., Academic Press, London (1982).

[37] Im JS, Woo SW, Jung MJ, Lee YS. Improved capacitance characteristics of electrospun ACFs by pore size control and vanadium catalyst. J Colloid Interface Sci, **327**, 115 (2008). http://dx.doi.org/10.1016/j.jcis.2008.08.030.

[38] Ravikovitch PI, Neimark AV. Characterization of nanoporous materials from adsorption and desorption isotherms. Colloids Surf A: Physicochem Eng Aspects, **187-188**, 11 (2001). http://dx.doi.org/10.1016/s0927-7757(01)00614-8.

[39] Celzard A, Albiniak A, Jasienko-Halat M, Mareche JF, Furdin G. Methane storage capacities and pore textures of active carbons undergoing mechanical densification. Carbon, **43**, 1990 (2005). http://dx.doi.org/10.1016/j.carbon.2005.03.022.

[40] Yeon SH, Osswald S, Gogotsi Y, Singer JP, Simmons JM, Fischer JE, Lillo-Rodenas MA, Linares-Solano A. Enhanced methane storage of chemically and physically activated carbide-derived carbon. J Power Sources, **191**, 560 (2009). http://dx.doi.org/10.1016/j.jpowsour.2009.02.019.

[41] Im JS, Park SJ, Kim TJ, Kim YH, Lee YS. The study of controlling pore size on electrospun carbon nanofibers for hydrogen adsorption. J Colloid Interface Sci, **318**, 42 (2008). http://dx.doi.org/10.1016/j.jcis.2007.10.024.